Received: 5 May 2021 | Revised: 25 June 2021 | Accepted: 2 July 2021

DOI: 10.1002/jhet.4340

ARTICLE

JOURNAL OF HETEROCYCLIC CHEMISTRY WILEY

Arylquinolinecarboxamides: Synthesis, *in vitro* and *in silico* studies against *Mycobacterium tuberculosis*

Fostino R. B. Bokosi[1] | **Richard M. Beteck**[1,2] | **Audrey Jordaan**[3] | **Ronnet Seldon**[4] | **Digby F. Warner**[3,5] | **Tendamudzimu Tshiwawa**[1] | **Kevin Lobb**[1] | **Setshaba D. Khanye**[1,6,7]

[1]Department of Chemistry, Faculty of Science, Rhodes University, Makhanda, South Africa

[2]Centre of Excellence for Pharmaceutical Sciences, North-West University, Potchefstroom, South Africa

[3]SAMRC/NHLS/UCT Molecular Mycobacteriology Research Unit, Department of Pathology, Faculty of Health Sciences, Institute of Infectious Disease and Molecular Medicine, University of Cape Town, Cape Town, South Africa

[4]SAMRC Drug Discovery and Development Unit, University of Cape Town, Cape Town, South Africa

[5]Wellcome Centre for Infectious Diseases Research in Africa, University of Cape Town, Cape Town, South Africa

[6]Centre for Chemico- and Biomedicinal Research, Rhodes University, Makhanda, South Africa

[7]Division of Pharmaceutical Chemistry, Faculty of Pharmacy, Rhodes University, Makhanda, South Africa

Correspondence
Setshaba D. Khanye, Division of Pharmaceutical Chemistry, Faculty of Pharmacy, Rhodes University, Makhanda 6140, South Africa.
Email: s.khanye@ru.ac.za

Fostino R. B. Bokosi, Department of Chemistry, Faculty of Science, Rhodes University, Makhanda 6140, South Africa.
Email: bokosifostino@gmail.com

Funding information
Malawi Goverment Scholarship Fund; South African Medical Research Council; Rhodes University; National Research Foundation, Grant/Award Number: SDK, Grant No. 107270

Abstract

A series of fourteen 6-substituted-2-(methoxyquinolin-3-yl) methyl)-*N*-(pyridin-3-ylmethyl) benzamides was prepared from commercially available anilines in five simple and convenient synthetic steps. The structures of all new products were confirmed by routine spectroscopic methods: IR, ^{1}H and ^{13}C NMR, and HRMS (electrospray ionization). The resulting arylquinolinecarboxamides were subjected to biological screening assay for *in vitro* inhibitory activity against *Mycobacterium tuberculosis* (*Mtb*) H37Rv strain. Several compounds exhibited modest antitubercular activity with compounds **8–11**, **15** and **19** exhibiting MIC_{90} values in the range of 32–85 μM. The antitubercular data suggested that inhibition of *Mtb* can be imparted by the introduction of a non-polar substituent on C-6 of the quinoline scaffold. Further, to understand the possible mode of action of the series, the reported compounds and bedaquiline were subjected to *in silico* docking studies against *Mtb*ATPase to determine their potential to interfere with the mycobacterial adenosine triphosphate (ATP) synthase. The results showed that these compounds have the potential to serve as antimycobacterial agents. *In silico* ADME pharmacokinetic prediction results showed the ability of these arylquinolinecarcboxamides to be absorbed, distributed, metabolized and excreted efficiently.

KEYWORDS

antitubercular, arylquinolinecarboxamides, *Mtb*ATPase, *Mycobacterium tuberculosis*

1 | INTRODUCTION

Tuberculosis (TB) is one of the oldest infectious diseases, which has claimed scores of human lives worldwide. TB is caused by *Mycobacterium tuberculosis* (*Mtb*). Despite a global reduction in TB mortality, 1.4 million people died from TB in 2019 [1]. The disease is currently treated using the first line regiment of four drugs, rifampicin (RIF), isoniazid (INH), pyrazinamide (PZA), ethambutol (EMT), which must be taken daily for a duration of at least six months [2]. The current clinical management of TB is complex, and the situation has been worsened by the emergence of multi-drug resistant TB (MDR-TB), a form of *Mtb* strains resistant to at least RIF and INH, and extensively drug resistance TB (XDR-TB), another form of MDR *Mtb* strains with additional resistance to at least one fluoroquinolone and one second-line injectable drug [3,4]. Both these TB resistant forms compromise the effectiveness of the existing therapy as well as control and clinical management of TB infections.

Quinoline nucleus represents an essential scaffold in many biologically active natural products and a variety of synthetic compounds with attractive pharmacological profiles [5]. A typical example is bedaquiline ((TMC207, Sirturo, Janssen Pharmaceuticals; Figure 1), a diarylquinoline (DARQ) which was recently approved under an accelerated programme for orphan drugs as an effective clinically approved drug reserved for MDR-TB alongside with other TB armaments [6–8]. It potently inhibits both drug-sensitive and drug-resistant *Mtb* by interfering with the mycobacterial adenosine triphosphate (ATP) synthase, an enzyme involved in ATP production in the bacterium [6,9–15]. The identification of bedaquiline as a new class of antimycobacterial drug with a novel mode of action has renewed interests to explore compounds containing the quinoline nucleus in a campaign to develop bioactive compounds capable of targeting different biochemical pathways within the microorganisms.

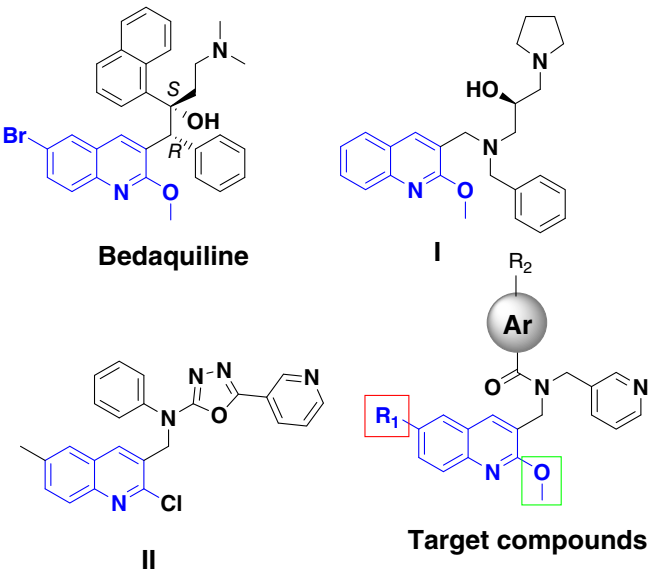

FIGURE 1 Chemical structures of bedaquiline and related quinoline derivatives showing activity against *Mtb*

In an attempt to identify new chemical entities, rationally designed novel arylquinolines as potential antitubercular agents by retaining the core unit of bedaquiline, 2-methoxyquinoline (drawn in blue), and its required 3D geometry were reported [16]. The synthesised compounds showed encouraging growth inhibition against *Mtb* H37Rv with MIC values in the range of 5–140 μM. Compound **I** (Figure 1) emerged as the most active member of the arylquinoline series with MIC value of 5.18 μM using a resazurin microtitre assay (REMA) plate method. In a separate study, a library of compounds containing a 2-chloroquinoline framework were synthesized and found to display superior growth inhibition against *Mtb* H37Rv [17]. Amongst the hits identified was compound **II**, which showed appreciable percentage viability inhibition of 96% against *Mtb*.

Considering the above accounts, we undertook an assemblage of a focused series of compounds containing the bedaquiline core; 2-methoxyquinoline as a main nucleus, while strategically varying substituents at position 6 of the quinoline scaffold as potential starting compounds for treatment of *Mtb*. The substituents R^1 and R^2 on the quinoline and benzoyl ring respectively were chosen in order to assess the influence that the electronic effects may have on the antimycobacterial activity. In this work, we report synthesis, spectroscopic characterization, and preliminary *in vitro* biological evaluation alongside *in silico* studies of a representative series of 2-(methoxyquinolin-3-yl) methyl)-*N*-(pyridin-3-ylmethyl) benzamides against *Mtb* H37Rv strain.

2 | RESULTS AND DISCUSSION

2.1 | Chemistry

Despite some limitations such as toxicity, bedaquline exhibits significant activity against *Mtb* by targeting the mycobacterial adenosine triphosphate (ATP) synthase, which is an essential enzyme in ATP production. Over the years, strategic modification of the bedaquiline structure to address some of observed limitations has led to several analogues showing significant antimycobacterial activity against *Mtb* [18]. In this study, we embarked on a rational design approach by retaining the 2-methoxyquinoline core structure of bedaquiline while modifying substituents at position 6 of the quinolone scaffold [19,20]. The targeted

compounds (Figure 1) were achieved following the synthetic route presented in Scheme 1. *N*-acylation of starting *para*-substituted anilines (**1a – d)** using the acetic anhydride–glacial acetic acid (1:1) at room temperature for 30 minutes yielded amides **2a–d**, which were obtained in 96–98% yields. Subsequent Vilsmeier-Haack cyclization of amides **2a–d** afforded key starting intermediates 6-substituted 2-chloroquinoline-3-carbaldehydes **3a–d**, which were sequentially treated with methanol/KOH to afford 2-methoxyquinoline derivatives **4a–d** in 60–70% yields [21,22]. The Schiff-base condensation reaction of aldehydes **4a–d** with 3-aminomethylpyridine in ethanol and catalytic amount of glacial acetic acid under refluxing conditions generated imine intermediates, which were reduced *in situ* using sodium borohydride at room temperature to give rise to amines **5a–d** in 62–70% yields. The final *N*-amidation step of **5a–d** was achieved by treatment with cold TEA and 4-DMAP at 0°C in the presence of selected benzoyl chlorides to afford carboxamides **6–19** with yields in the range of 41–72%. Structures of critical intermediate compounds (**2a–d**, **3a–d**, **4a–d** and **5a–d**) and corresponding target arylquinolinecarboxamide derivatives (**6–19**) were confirmed using various spectroscopic techniques (IR, ^{1}H-NMR, ^{13}C-NMR and HRMS). A comprehensive spectral data is presented as an Electronic Supplementary Information (**ESI**) file.

The FT-IR of all target compounds showed consistent broad intense stretch bands in the range ~ 1617–1628 cm^{-1}, which are assignable to –C=O of amide unit. The disappearance of the characteristic strong band *ca* 3320–3050 cm^{-1} of the N–H group confirmed successful conversion from secondary amine to the amide functional group. Various aromatic/hetero-aromatic ^{1}H signals were observed between δ 8.60 and 6.90 ppm. The most deshielded protons, found in the range 8.57–8.43 ppm, were assignable to the protons adjacent to nitrogen in the 3-(aminomethyl) pyridine scaffold. Th intense singlet signal observed between 7.94 and 8.04 ppm in all the compounds was due to the proton on C4 of the quinoline ring. The ^{1}H-NMR spectra of compounds reveal expected methylene protons integrating for four. More importantly, ^{1}H and ^{13}C NMR spectra of target arylquinolinecarboxamides displayed duplicate and/or broad proton signals at 298 K (see electronic supplementary information **Figure S39**) attributed to possible existence of the rotational isomers caused by the restricted rotation around the C–N amide bond known as rotamers [23–27]. The assignment of signals was facilitated by conducting NMR experiments of each compound in DMSO-d_6 at variable temperatures ranging from 298 to 353 K [26,28–30]. A characteristic ^{13}C NMR signal appearing around δ 171.9–171.0 ppm indicated the presence of carbonyl carbon (C=O) of the amide unit in the target compounds. The ^{13}C NMR spectra of most prepared compounds showed the apparent absence of expected *N*-methylene signals and this phenomenon is attributed to site-exchange line-broadening effects [31]. Additionally, high-resolution mass spectroscopy (HRMS) analysis for all the compounds unequivocally confirmed the existence of molecular ions consistent with molecular weights of prepared compounds, thereby confirming the respective chemical structures.

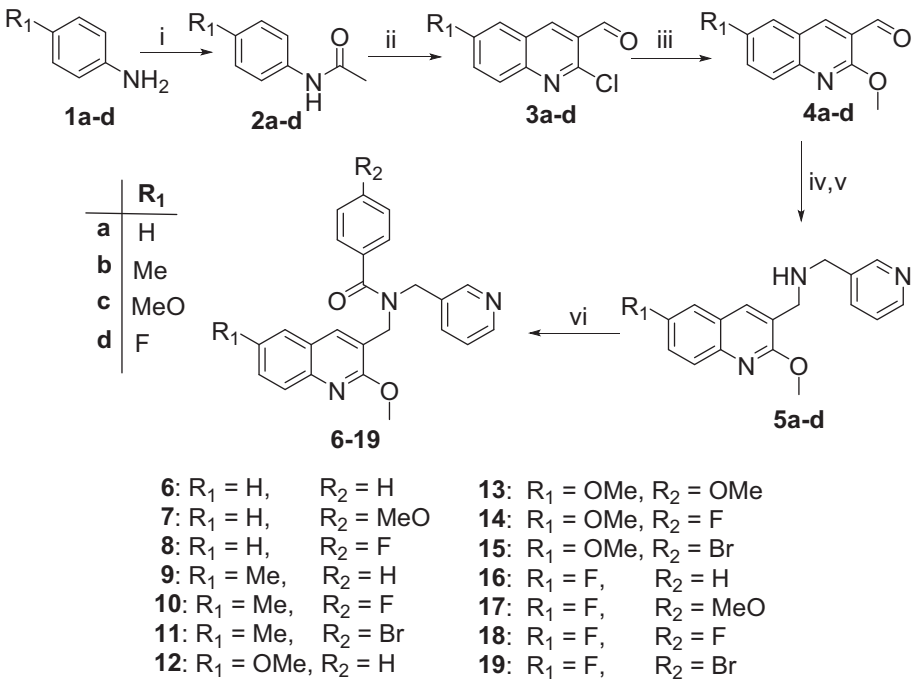

SCHEME 1 Synthetic route for the synthesis of arylquinolinecarboxamide derivatives **6–19**. *Reagents and conditions*: (i) Ac_2O, AcOH, r.t, 30 min; (ii) DMF–$POCl_3$, 80°C, 5–18 h; (iii) MeOH, KOH, reflux, 3–4 h; (iv) 3-Picolylamine, EtOH, AcOH (cat), reflux, 12 h; (v) EtOH, sodium borohydride, rt, 6 h; (vi) substituted benzoyl chlorides, DCM, TEA, 4-DMAP (cat), 0°C, 12 h

2.2 | Antimycobacterial activity

Compounds **6–19** were evaluated for potential *in vitro* antitubercular activity using a broth microdilution assay against H37Rv, the drug susceptible strain of *Mtb* with rifampicin included as a standard drug. The antitubercular activities are reported as the minimum inhibitory concentration (MIC_{90}), which is a required concentration to inhibit 90% of mycobacterial growth. Antitubercular activity data of target compounds is presented in Table 1. The data revealed that the structural variation at position 6 (R^1) of the quinoline ring and the functionalization of the benzoyl scaffold (R^2) to some extent influenced the antitubercular activity. Analysis of the substituents at position 6 of the quinoline nucleus suggested that a methyl substituent promoted antitubercular activity better than methoxy, fluoro and non-substituted derivatives. For example, modest activity was observed for compounds **9** (MIC_{90}; 84.2 μM), **10** (MIC_{90}; 32.5 μM) and **11** (MIC_{90}; 40.3 μM) – all bearing a methyl substituent at position 6 of the quinoline ring. Similarly, compounds **11** (MIC_{90}; 40.3 μM), **15** (MIC_{90}; 55.1 μM) and **19** (MIC_{90}; 50.1 μM) which contain a combination of methyl, methoxy and fluoro substituents at position 6 coupled with the carboxamide aromatic ring bearing bromine at the para position were at most moderately active. It is important to note that compound **11** (MIC_{90}; 40.3 μM), which bears both the favored 6-methyl group on position 6 of the quinoline ring and a bromine group on para position of the benzoyl moiety, proved to be one of the most active compounds of the series as anticipated from the preliminary structure activity relationships (SAR).

2.3 | *In silico* studies

An *in silico* binding interaction study of bedaquiline using the homology model of *Mtb*ATPase was conducted to gain better insight into the key residues involved in the binding of bedaquiline and functioning of *Mtb*ATPase. The homology model of *Mtb*ATPase DARQ binding site scored very well in ERRAT (see electronic supplementary information **Figures 40S** and **41S**) with all the residues below the error region and only a few residues appeared above the warning site. The molecular docking values measure the fitness of ligand into the binding site of a protein or an enzyme, and more negative docking value is an indication of the better fitness of the molecule at the binding site of the protein [32]. The result of the docking analysis from this study showed the standard drug (Bedaquiline) exhibited the best binding fitness at the binding site of the *Mtb*ATPase with a docking score of −7.934 kcal/mol. The majority of docked ligands had the docking score that is within the same range as that of the known inhibitor bedaquiline (Table 1). All docking scores less than −5 kcal/mol indicate good affinity between the ligands and the target receptor. As shown in Figure 2, there are several intramolecular interactions observed between ligands and receptor residues. These interactions include conventional intramolecular hydrogen bonds, pi-pi stacking and pi-cation. All these interactions are a good indicator of binding affinity between the ligands and the receptor [33].

In drug discovery, several potential therapeutic agents fail to enter the clinical trials due to their unfavorable drug-likeliness and poor ADME properties [34]. Thus, for an efficient drug molecule, a compound should possess desirable high biological activity, low toxicity and appropriate ADME property profile. In an attempt to assess drug-likeliness and ADME properties, a computational study of synthesized compounds (**6–19**) was performed and values obtained are tabulated in Table 2. The observed drug-like properties and analysis of *in silico* ADME prediction suggest that these compounds are exhibiting acceptable ADME profile despite some of the compounds within the series showing predicted octanol/water partition coefficient $QPlogP_{o/w} > 5.0$ (Table 2).

3 | EXPERIMENTAL

All chemicals and reagents used were purchased from Merck® and where necessary, they were purified according to the methods reported in literature [36]. The reaction progress was monitored by thin layer chromatography (TLC) using Merck 60-F254 silica gel plates supported on aluminum and viewed under UV light. The purification of synthesised compounds was carried out using a silica gel column chromatography using Merck Kieselgel 60 Å: 70–230 (0.068–0.2 mm) silica gel mesh. NMR spectra were recorded on Bruker Fourier 300 MHz, AMX 400 MHz or Biospin 600 MHz spectrometers in $CDCl_3$ or DMSO-d_6 and calibrated using solvents signals [δ_H: 7.26 ppm for $CDCl_3$ and 2.50 ppm for DMSO-d_6; δ_C: 77.0 ppm for $CDCl_3$ and 39.4 ppm for DMSO-d_6]. The spectra were processed using processed using MestReNova Software version 5.3.2–4936 or Bruker Topspin 3.5 software®. High-resolution electrospray ionization mass spectrometry data (HRMS) were recorded on a Waters Synapt G2 quadrupole time-of-flight (QTQF) mass spectrometer (Stellenbosch University, Stellenbosch, South Africa). The IR spectra were recorded on PerkinElmer 100 FT-IR Spectrometer in the mid-IR range (640–4000 cm^{-1}). Melting points were measured using Stuart melting point apparatus SMP30 and were reported uncorrected.

TABLE 1 *In vitro* antitubercular evaluation of compounds **6–19** against drug susceptible *Mtb* H37Rv and in comparison, with the standard drug rifampicin and docking results

Compound	Structure	[a]MIC90 μM 7D7H9LUCASTX	Docking score (kcal/mol)	Compound	Structure	[a]MIC90 μM 7D7H9LUCASTX	Docking score (kcal/mol)
Bedaquiline	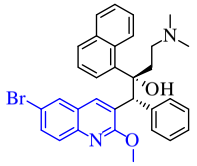	n.d.	−7.934	**13**	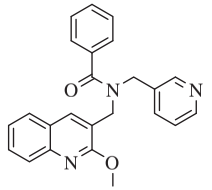	>125	−7.454
6	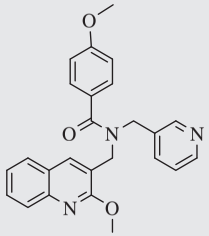	>125	−6.954	**14**	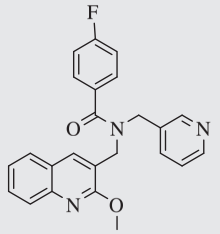	>125	−6.590
7	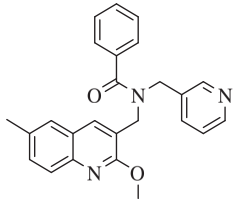	>125	−7.713	**15**	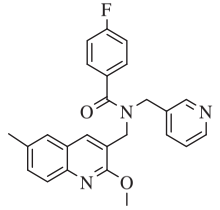	55.1	−6.018
8	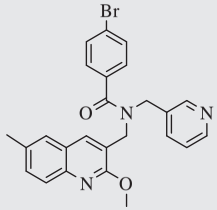	67.3	−6.480	**16**	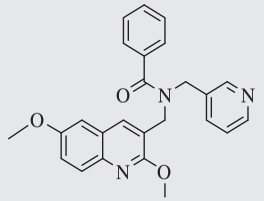	>125	−7.067
9	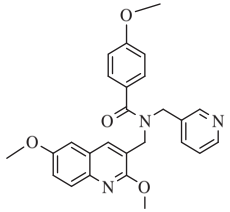	84.2	−6.600	**17**	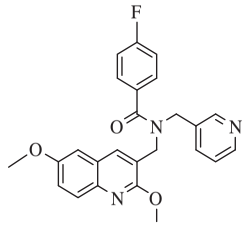	>125	−6.212

(Continues)

TABLE 1 (Continued)

Compound	Structure	[a]MIC90 μM 7D7H9LUCASTX	Docking score (kcal/mol)	Compound	Structure	[a]MIC90 μM 7D7H9LUCASTX	Docking score (kcal/mol)
10	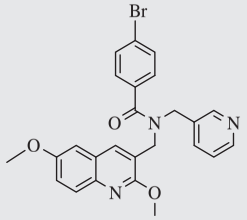	32.5	−6.212	**18**	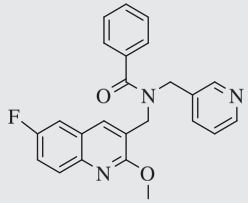	>125	−6.363
11	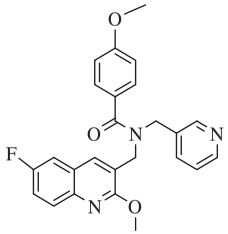	40.3	−5.980	**19**	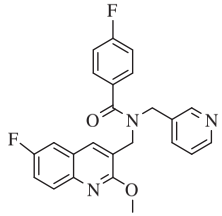	50.1	−5.971
12	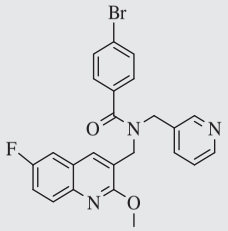	>125	−6.223	**RMP**	-	0.075	-

Note: RMP = rifampicin was used as positive control.

[a]Data are the average and SD of two independent experiments. n.d. = not determined.

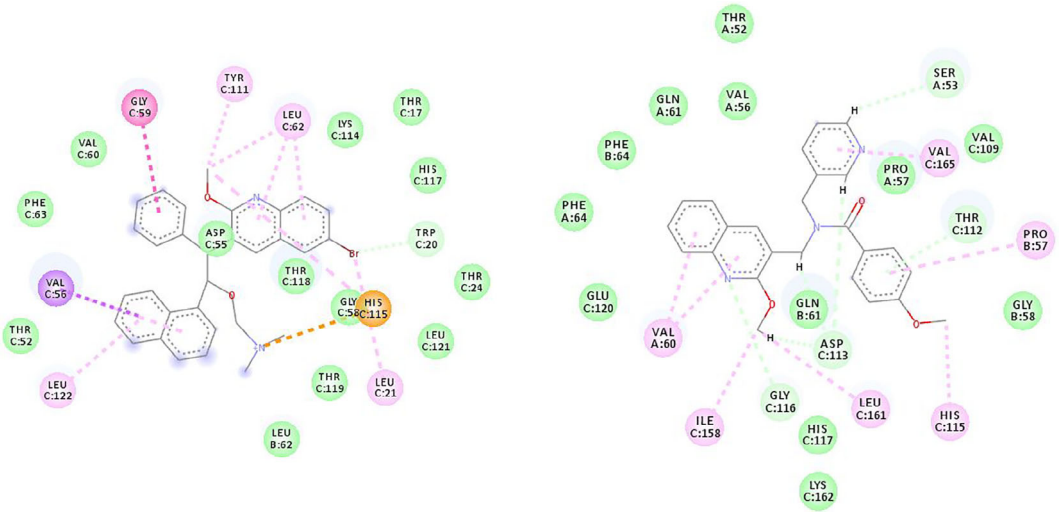

FIGURE 2 Bedaquiline and the best docked ligand **7** receptor ligand interactions

TABLE 2 The drug likeliness and *in silico* ADME properties of all the synthesized compounds

Compound	[a]QPlogHERG	[b]Mw	[c]QPlogPo/w	[d]QPlogS	[e]QPlogBB	[f]QPPMDCK	[g]%Human OralAbsorption	[h]Rule of 5
6	4.0	413.475	4.59	−4.53	−0.449	1326.645	100	0
7	3.8	383.449	4.77	−5.19	−0.406	1389.388	100	0
8	4.0	401.439	5.01	−5.50	−0.306	2406.163	100	1
9	4.3	397.476	5.23	−5.73	−0.364	1554.356	100	1
10	4.5	415.466	5.09	−5.49	−0.236	2779.078	100	1
11	5.2	476.372	5.69	−6.51	−0.186	4119.007	100	1
12	4.0	413.475	4.85	−5.19	−0.429	1533.986	100	0
13	4.3	443.501	4.67	−4.67	−0.525	1331.025	100	0
14	4.3	431.465	5.09	−5.56	−0.318	2780.182	100	1
15	5.0	492.371	5.24	−5.34	−0.167	4478.546	100	1
16	4.2	431.465	4.83	−4.88	−0.338	2403.837	100	0
17	4.2	419.43	5.25	−5.88	−0.197	4354.318	100	1
18	3.9	401.439	5.15	−5.79	−0.29	2619.793	100	1
19	4.5	480.335	5.561	−6.328	−0.135	6263.976	100	1

[a]QPlogHERG: Predicted IC_{50} value for blockage of HERG K+ channels.
[b]Mw: Molecular weight of the molecule.
[c]QPlogPo/w: Predicted octanol/water partition coefficient.
[d]QPlogS: Predicted aqueous solubility.
[e]QPlogBB: Predicted brain/blood partition coefficient.
[f]QPPMDCK: Predicted apparent MDCK cell permeability in nm/sec.
[g]%HumanOralAbsorption: Predicted human oral absorption on 0–100% scale.
[h]Rule of 5: Denotes the number of violations of Lipinski's rule of five. Compounds that satisfy these rules are considered drug like [35].

3.1 | General procedure for the synthesis of target compounds (6–19)

Target compounds were synthesized by employing an efficient amide coupling protocol [37]. To a suitable secondary amines **5a**–**d** (1.0 equiv), triethylamine (2.0 equiv) and few granules of catalytic 4-DMAP were dissolved in 10 mL of CH_2Cl_2. The flask was cooled down to 0°C and appropriate benzoyl chloride (2.0 equiv) was added dropwise. The resulting mixture was stirred overnight at room temperature. The reaction was quenched with water (5 mL) extracted with CH_2Cl_2 (3 × 15 mL). The combined organic layers washed with brine (20 mL), dried (Na_2SO_4) and concentrated under reduced pressure.

The crude product was purified by silica gel column chromatography (EtOAc:Hexane 2:8) to yield desired benzamides **6–19**. Characterization of synthesized compounds is given below.

3.1.1 | *N-([2-Methoxyquinolin-3-yl] methyl)-N-(pyridin-3-ylmethyl) benzamide* (6)

White crystalline solid. Yield = 71%; M.p: 147–149 °C; ν_{max}/cm^{-1} 1626 (C=O); ^{1}H NMR (400 MHz, $CDCl_3$): δ_H = 8.51–8.33 (2H, m, overlapping H-8′ and H-9′), 8.25–7.93 (1H, m, H-4), 7.79–7.77 (1H, m, H-8), 7.75–7.63 (2H, m, H-5, H-6′), 7.57–7.56 (1H, m, H-5″), 7.42–7.38 (2H, m, H-3″), 7.33–7.30 (4H, m, H-6, H-7, H-4″), 7.23–7.22 (1H, m, H-7′), 4.72 (2H, s, CH_2, H-3′), 4.59–4.53(2H, m, CH_2, H-4′), 4.07–3.98 (3H, m, OCH_3); ^{13}C NMR (100 MHz, $CDCl_3$) δ_C = 172.9, 159.9, 149.6, 149.1, 146.0, 138.1, 136.1, 135.7, 132.8, 130.1, 129.7, 128.6, 127.3, 127.0, 126.7, 124.9, 124.6, 123.7, 120.5, 53.6, 48.1, 45.7; *m/z* (ESI) calcd for $C_{24}H_{22}N_3O_2$ [M + H]$^+$: 384.1712, found 384.1714.

3.1.2 | *4-Methoxy-N-([2-methoxyquinolin-3-yl]methyl)-N-(pyridin-3-ylmethyl) benzamide* (7)

White crystalline solid. Yield = 65%; M.p: 142–144 °C; ν_{max}/cm^{-1}: 1625 (C=O); ^{1}H NMR (600 MHz, DMSO-d_6 at 328 K): δ_H = 8.46–8.42 (2H, m, overlapping H-8′ and H-9′), 8.10 (1H, s, H-4), 7.93 (1H, d, J = 7.8 Hz, H-8), 7.77–7.76 (1H, m, H-5), 7.68 (1H, bs, H-6′), 7.66–7.64 (1H, m, H-7), 7.50 (2H, d, J = 8.1 Hz, H-3″), 7.46–7.43 (1H, m, H-6), 7.33 (1H, dd, J = 7.5, 4.9 Hz, H-7′), 6.97 (2H, d, J = 8.1 Hz, H-4″), 4.71 (2H, s, CH_2, H-3′), 4.61 (2H, s, CH_2, H-4′), 3.93 (3H, s, OCH_3), 3.77 (3H, s, OCH_3); ^{13}C NMR (150 MHz, DMSO-d_6 at 328 K): δ_C = 171.9, 160.8, 160.2, 149.3, 148.8, 145.6, 136.7, 135.5, 133.5, 130.0, 129.0, 128.5, 128.2, 126.8, 125.3, 124.7, 124.0, 121.3, 114.2, 55.7, 53.8; *m/z* (ESI) calcd for $C_{25}H_{24}N_3O_3$ [M + H]$^+$: 414.1818, found 414.1813.

3.1.3 | *4-Fluoro-N-([2-methoxyquinolin-3-yl] methyl)-N-(pyridin-3-ylmethyl) benzamide* (8)

White crystalline solid. Yield = 55%; M.p: 122–124 °C; ν_{max}/cm^{-1}: 1632 (C=O); ^{1}H NMR (600 MHz, DMSO-d_6 at 328 K): δ_H = 8.46–8.42 (2H, m, overlapping H-8′ and H-9′), 8.10 (1H, s, H-4), 7.93 (1H, d, J = 7.9 Hz, H-8), 7.77–7.76 (1H, m, H-5), 7.68–7.67 (1H, m, H-6′), 7.66–7.64 (1H, m, H-7), 7.62–7.59 (2H, m, H-3″), 7.46–7.43 (1H, m, H-6), 7.32 (1H, dd, J = 7.6, 4.9 Hz, H-7′), 7.26 (2H, t, J = 8.7 Hz, H-4″), 4.70 (2H, s, CH_2, H-3′), 4.60 (2H, s, CH_2, H-4′), 3.93 (3H, s, OCH_3); ^{13}C NMR (150 MHz, DMSO-d_6 at 328 K): δ_C = 171.1, 163.1 (d, J = 246.9 Hz), 160.2, 149.3, 148.9, 145.7, 137.1, 135.6, 133.4, 133.0 (d, J = 3.3 Hz), 129.9, 129.7 (d, J = 8.6 Hz), 128.2, 126.8, 125.3, 124.7, 123.9, 121.1, 115.9 (d, J = 21.5 Hz), 53.7; *m/z* (ESI) calcd for $C_{24}H_{21}N_3O_2F$ [M + H]$^+$: 402.1618, found 402.1623.

3.1.4 | *N-([2-Methoxy-6-methylquinolin-3-yl] methyl)-N-(pyridin-3-ylmethyl) benzamide* (9)

White crystalline solid. Yield = 72%; M.p: 136–138 °C; ν_{max}/cm^{-1} 1621 (C=O); ^{1}H NMR (300 MHz, $CDCl_3$): δ_H = 8.56–8.51 (2H, m, overlapping H-8′ and H-9′), 7.76–7.72 (3H, m, H-4, H-8, H-6′), 7.51 (1H, s, H-5), 7.49–7.44 (3H, m, H-3″, H-5″), 7.42–7.37 (3H, m, H-7, H-4″), 7.31–7.26 (1H, m, H-7′), 4.78 (2H, bs, CH_2, H-3′), 4.52 (2H, bs, CH_2, H-4′), 3.97 (3H, bs, OCH_3), 2.51 (3H, s, CH_3); ^{13}C NMR (75 MHz, $CDCl_3$): δ_C = 172.8, 159.6, 149.5, 149.1, 144.3, 136.1, 135.7, 135.3, 134.6, 134.1, 132.8, 131.7, 130.0, 128.6, 126.7, 126.5, 124.9, 123.7, 120.3, 53.4, 48.1, 45.7, 21.3; *m/z* (ESI) calcd for $C_{25}H_{24}N_3O_2$ [M + H]$^+$: 398.1869, found 398.1878.

3.1.5 | *4-Fluoro-N-([2-methoxy-6-methylquinolin-3-yl]methyl)-N-(pyridin-3-ylmethyl) benzamide* (10)

White crystalline solid. Yield = 49%; M.p: 139–141 °C; ν_{max}/cm^{-1} 1632 (C=O); ^{1}H NMR (600 MHz, DMSO-d_6 at 308 K): δ_H = 8.47–8.44 (2H, m, overlapping H-8′ and H-9′), 7.99 (1H, s, H-4), 7.71–7.63 (3H, m, H-6′, H-5, H-8), 7.63–7.58 (2H, m, H-3″), 7.48 (1H, dd, J = 8.5, 1.7 Hz, H-7), 7.32 (1H, dd, J = 7.6, 4.9 Hz, H-7′), 7.26 (2H, t, J = 8.6 Hz, H-4″), 4.68 (2H, s, CH_2, H-3′), 4.59 (2H, s, CH_2, H-4′), 3.91 (3H, s, OCH_3), 2.46 (3H, s, CH_3); ^{13}C NMR (150 MHz, DMSO-d_6 at 308 K): δ_C = 171.1, 163.1 (d, J = 246.9 Hz), 159.7, 149.3, 148.8, 144.0, 136.5, 135.6, 133.9, 133.4, 133.0 (d, J = 3.2 Hz), 131.8, 129.6 (d, J = 8.6 Hz), 127.2, 126.6, 125.2, 123.9, 120.9, 115.9 (d, J = 21.7 Hz), 53.6, 49.0, 46.6, 21.3; *m/z* (ESI) calcd for $C_{25}H_{23}N_3O_2F$ [M + H]$^+$: 416.1774, found 416.1779.

3.1.6 | *4-Bromo-N-([2-methoxy-6-methylquinolin-3-yl]methyl)-N-(pyridin-3-ylmethyl) benzamide* (11)

White crystalline solid. Yield = 42%; M.p: 114–116 °C; ν_{max}/cm^{-1} 1621 (C=O); ^{1}H NMR (600 MHz, DMSO-d_6 at 308 K): δ_H = 8.46–8.44 (2H, m, overlapping H-8′ and H-9′), 7.98 (1H, s, H-4), 7.70–7.62 (5H, m, H-6′, H-5, H-8, H-

3″), 7.50–7.47 (3H, m, H-7, H-4″), 7.34–7.30 (1H, m, H-7′), 4.68 (2H, s, CH_2, H-3′), 4.56 (2H, s, CH_2, H-4′), 3.90 (3H, s, OCH_3), 2.46 (3H, s, CH_3); ^{13}C NMR (150 MHz, DMSO-d_6 at 308 K): δ_C = 171.0, 159.6, 149.3, 148.9, 144.0, 135.7, 135.2, 133.9, 131.9, 129.3, 129.2, 127.2, 127.1, 126.6, 125.2, 123.9, 123.5, 121.0, 120.7, 53.6, 46.6, 44.0, 21.3; *m/z* (ESI) calcd for $C_{25}H_{23}N_3O_2Br$ [M + H]$^+$: 476.0974, found 476.0972.

3.1.7 | *N-([2,6-Dimethoxyquinolin-3-yl] methyl)-N-(pyridin-3-ylmethyl) benzamide* (12)

White crystalline solid. Yield = 70%; M.p: 148–150 °C; ν_{max}/cm^{-1} 1628 (C=O); ^{1}H NMR (600 MHz, DMSO-d_6 at 328 K): δ_H = 8.47–8.44 (2H, m, overlapping H-8′ and H-9′), 8.04 (1H, s, H-4), 7.67–6.66 (2H, m, H-6′, H-8), 7.52 (2H, bs, H-3″), 7.47–7.41 (4H, m, H-5, H-4″ H-5″), 7.34 (1H, dd, *J* = 7.8, 4.8 Hz, H-7′), 7.29 (1H, dd, *J* = 9.0, 2.9 Hz, H-7), 4.70 (2H, s, CH_2, H-3′), 4.56 (2H, s, CH_2, H-4′), 3.91–3.87 (6H, m, 2 × OCH_3); ^{13}C NMR (150 MHz, DMSO-d_6 at 328 K): δ_C = 172.0, 158.7, 156.3, 149.3, 148.9, 140.9, 136.6, 136.0, 135.5, 133.3, 130.1, 128.9, 128.1, 127.0, 126.1, 124.0, 121.3, 121.2, 107.4, 55.9, 53.6; *m/z* (ESI) calcd for $C_{25}H_{24}N_3O_3$ [M + H]$^+$: 414.1818, found 414.1816.

3.1.8 | *N-([2,6-Dimethoxyquinolin-3-yl] methyl)-4-methoxy-N-(pyridin-3-ylmethyl) benzamide* (13)

White crystalline solid. Yield = 64%; M.p: 99–101 °C; ν_{max}/cm^{-1} 1613 (C=O); ^{1}H NMR (600 MHz, DMSO-d_6 at 328 K): δ_H = 8.46–8.43 (2H, m, overlapping H-8′ and H-9′), 8.04 (1H, s, H-4), 7.69–7.66 (2H, m, H-6′, H-8), 7.49 (2H, d, *J* = 7.7 Hz, H-3″), 7.42 (1H, d, *J* = 2.6 Hz, H-5), 7.34 (1H, dd, *J* = 7.4, 4.9 Hz, H-7′), 7.28 (1H, dd, *J* = 9.0, 2.6 Hz, H-7), 6.97 (2H, d, *J* = 7.7 Hz, H-4″), 4.69 (2H, s, CH_2, H-3′), 4.57 (2H, s, CH_2, H-4′), 3.89–3.85 (6H, s, 2 × OCH_3), 3.76 (3H, s, OCH_3); ^{13}C NMR (150 MHz, DMSO-d_6 at 328 K): δ_C = 171.9, 160.8, 158.7, 156.3, 154.8, 149.4, 148.9, 140.9, 135.7, 133.5, 129.0, 128.5, 128.1, 126.1, 124.0, 121.4, 121.3, 114.2, 107.3, 55.9, 55.7, 53.6; *m/z* (ESI) calcd for $C_{26}H_{26}N_3O_4$ [M + H]$^+$: 444.1923, found 444.1920.

3.1.9 | *N-([2,6-Dimethoxyquinolin-3-yl] methyl)-4-fluoro-N-(pyridin-3-ylmethyl) benzamide* (14)

White crystalline solid. Yield = 51%; M.p: 106–108 °C; ν_{max}/cm^{-1} 1632 (C=O); ^{1}H NMR (600 MHz, DMSO-d_6 at 328 K): δ_H = 8.47–8.44 (2H, m, overlapping H-8′ and H-9′), 8.03 (1H, s, H-4), 7.68–7.67 (2H, m, H-6′, H-8), 7.63–7.58 (2H, m, H-3″), 7.40 (1H, s, H-5), 7.35–7.32 (1H, m, H-7′), 7.30 (1H, d, *J* = 9.0 Hz, H-7), 7.26 (2H, t, *J* = 8.3 Hz, H-4″), 4.70 (2H, s, CH_2, H-3′), 4.59 (2H, s, CH_2, H-4′), 3.91–3.89 (6H, m, 2 × OCH_3); ^{13}C NMR (150 MHz, DMSO-d_6 at 328 K): δ_C = 171.1, 163.1 (d, *J* = 246.6 Hz), 158.8, 156.4, 149.3, 148.9, 141.0, 136.1, 135.6, 133.3, 133.0 (d, *J* = 3.4 Hz), 129.6 (d, *J* = 8.1 Hz), 128.1, 126.1, 123.9, 121.3, 121.1, 115.9 (d, *J* = 21.9 Hz), 107.5, 56.0, 53.5; *m/z* (ESI) calcd for $C_{25}H_{23}N_3O_3F$ [M + H]$^+$: 432.1723, found 432.1719.

3.1.10 | *4-Bromo-N-([2,6-dimethoxyquinolin-3-yl]methyl)-N-(pyridin-3-ylmethyl) benzamide* (15)

White crystalline solid. Yield = 47%; M.p: 107–109 °C; ν_{max}/cm^{-1} 1621 (C=O); ^{1}H NMR (600 MHz, DMSO-d_6 at 328 K): δ_H = 8.46–8.44 (2H, m, overlapping H-8′ and H-9′), 8.00 (1H, s, H-4), 7.68–7.66 (2H, m, H-8, H-6′), 7.63 (2H, d, *J* = 7.9 Hz, H-3″), 7.48 (2H, d, *J* = 7.9 Hz, H-4″), 7.38 (1H, d, *J* = 2.6 Hz, H-5), 7.31 (1H, dd, *J* = 7.5, 4.9 Hz, H-7′), 7.28 (1H, dd, *J* = 9.0, 2.7 Hz, H-7), 4.68 (2H, s, CH_2, H-3′), 4.56 (2H, s, CH_2, H-4′), 3.93–3.86 (6H, m, 2 × OCH_3); ^{13}C NMR (150 MHz, DMSO-d_6 at 328 K) δ_C = 171.0, 158.8, 156.4, 149.3, 148.9, 141.0, 136.3, 135.8, 131.9, 129.2, 128.1, 126.1 (2C), 123.9, 123.5, 121.3, 121.0 (2C), 107.5, 56.0, 53.5; *m/z* (ESI) calcd for $C_{25}H_{23}N_3O_3Br$ [M + H]$^+$: 492.0931, found 492.0927.

3.1.11 | *N-([6-Fluoro-2-methoxyquinolin-3-yl] methyl)-N-(pyridin-3-ylmethyl) benzamide* (16)

White crystalline solid. Yield = 69%; M.p: 127–129 °C; ν_{max}/cm^{-1}: 1636 (C=O); ^{1}H NMR (300 MHz, $CDCl_3$): δ_H = 8.55–8.33 (2H, m, overlapping H-8′ and H-9′), 7.89–7.87 (1H, m, H-4), 7.75–7.65 (1H, m, H-8), 7.59–7.53 (1H, m, H-6′), 7.46–7.25 (7H, m, H-5, H-7, H-3″, H-4″, H-5″), 7.25–7.19 (1H, m, H-7′), 4.74–4.60 (2H, m, CH_2, H-3′), 4.55–4.46 (2H, m, CH_2, H-4′), 3.92–3.89 (3H, m, OCH_3); ^{13}C NMR (75 MHz, $CDCl_3$): δ_C = 172.2, 159.5, 159.2 (d, *J* = 242.9 Hz), 149.5, 149.2, 142.8, 136.1, 135.5, 134.9, 132.5, 130.1, 129.0 (d, *J* = 7.6 Hz), 128.6, 126.7, 125.3 (d, *J* = 5.2 Hz), 123.7, 121.6, 119.1 (d, *J* = 23.4 Hz), 110.8 (d, *J* = 22.4 Hz), 53.6, 48.1, 45.8; *m/z* (ESI) calcd for $C_{24}H_{21}N_3O_2F$ [M + H]$^+$: 402.1618, found 402.1619.

3.1.12 | *N-([6-Fluoro-2-methoxyquinolin-3-yl] methyl)-4-methoxy-N-(pyridin-3-ylmethyl) benzamide* (17)

White crystalline solid. Yield = 41%; M.p: 129–131 °C; ν_{max}/cm^{-1} 1617 (C=O); ^{1}H NMR (600 MHz, DMSO-d_6 at

328 K): δ_H = 8.46–8.42 (2H, m, overlapping H-8′ and H-9′), 8.09 (1H, s, H-4), 7.79 (1H, dd, J = 9.1, 5.3 Hz, H-8), 7.74 (1H, dd, J = 9.4, 3.0 Hz, H-5), 7.66 (1H, d, J = 7.7 Hz, H-6′), 7.52 (1H, td, J = 9.1, 3.0 Hz, H-7), 7.48 (2H, d, J = 8.5 Hz, H-3″), 7.31 (1H, dd, J = 7.7, 4.8 Hz, H-7′), 6.97 (2H, d, J = 8.5 Hz, H-4″), 4.69 (2H, s, CH_2, H-3′), 4.60 (2H, s, CH_2, H-4′), 3.93 (3H, s, OCH_3), 3.77 (3H, s, OCH_3); ^{13}C NMR (150 MHz, DMSO-d_6 at 328 K): δ_C = 171.9, 160.8, 159.9, 159.0 (d, J = 241.6 Hz), 149.3, 148.9, 142.6, 136.2, 135.6, 133.5, 129.1 (d, J = 8.9 Hz), 129.0, 128.5, 125.9 (d, J = 10.3 Hz), 123.9, 122.5, 119.1 (d, J = 25.1 Hz), 114.3, 111.7 (d, J = 22.2 Hz), 55.7, 53.8; *m/z* (ESI) calcd for $C_{25}H_{23}N_3O_3F$ $[M + H]^+$: 432.1723, found 432.1721.

3.1.13 | *4-Fluoro-N-([6-fluoro-2-methoxyquinolin-3-yl]methyl)-N-(pyridin-3-ylmethyl) benzamide* (18)

White crystalline solid. Yield = 43%; M.p: 109–111 °C; ν_{max}/cm^{-1} 1625 (C=O); ^1H NMR (600 MHz, DMSO-d_6 at 328 K): δ_H = 8.46–8.42 (2H, m, overlapping H-8′ and H-9′), 8.11 (1H, s, H-4), 7.79 (1H, dd, J = 8.8, 5.3 Hz, H-8), 7.74 (1H, dd, J = 7.6, 2.0 Hz, H-5), 7.67 (1H, bs, H-6′), 7.63–7.58 (2H, m, H-3″), 7.52 (1H, td, J = 8.8, 2.9 Hz, H-7), 7.31 (1H, dd, J = 7.6, 4.8 Hz, H-7′), 7.26 (2H, t, J = 8.7 Hz, H-4″), 4.70 (2H, s, CH_2, H-3′), 4.61 (2H, s, CH_2, H-4′), 3.93 (3H, s, OCH_3); ^{13}C NMR (150 MHz, DMSO-d_6 at 328 K): δ_C = 171.2, 163.1 (d, J = 247.1 Hz), 159.9, 159.0 (d, J = 241.6 Hz), 149.3, 148.9, 142.6, 136.4, 135.6, 133.3, 132.9 (d, J = 3.2 Hz), 129.6 (d, J = 8.5 Hz), 129.1 (d, J = 9.0 Hz), 125.8 (d, J = 9.8 Hz), 123.9, 122.3, 119.2 (d, J = 24.8 Hz), 115.9 (d, J = 21.8 Hz), 111.7 (d, J = 22.2 Hz), 54.8, 53.8; *m/z* (ESI) calcd for $C_{24}H_{20}N_3O_2F_2$ $[M + H]^+$: 420.1524, found 420.1525.

3.1.14 | *4-Bromo-N-([6-fluoro-2-methoxyquinolin-3-yl]methyl)-N-(pyridin-3-ylmethyl) benzamide* (19)

White crystalline solid. Yield = 46%; M.p: 143–145 °C; ν_{max}/cm^{-1}: 1636 (C=O); ^1H NMR (600 MHz, DMSO-d_6 at 328 K): δ_H = 8.45–8.43 (2H, m, overlapping H-8′ and H-9′), 8.11 (1H, s, H-4), 7.81–7.48 (8H, m, H-6′, H-8, H-3″, H-5, H-7, H-4″), 7.35–7.28 (1H, m, H-7′), 4.69 (2H, s, CH_2, H-3′), 4.57 (2H, s, CH_2, H-4′), 3.91 (3H, s, OCH_3); ^{13}C NMR (150 MHz, DMSO-d_6 at 328 K): δ_C = 171.1, 159.8, 158.9 (d, J = 241.6 Hz), 149.5, 148.9, 142.6, 136.6, 135.7, 133.4, 131.9, 129.2, 129.1 (d, J = 9.0 Hz), 125.8 (d, J = 8.7 Hz), 125.1, 123.9, 123.5, 122.1, 119.2 (d, J = 21.8 Hz), 111.7 (d, J = 22.1 Hz), 53.8, 48.8, 46.4; *m/z* (ESI) calcd for $C_{24}H_{20}N_3O_2FBr$ $[M + H]^+$: 480.0723, found 480.0733.

3.2 | *In vitro* antimycobacterial screening assay

The minimum inhibitory concentration (MIC) was determined using the standard broth microdilution method. Briefly, a 10 mL culture of *Mycobacterium tuberculosis* pMSp12: GFP [38–40] was grown to an optical density (OD600) of 0.6–0.7 in Middlebrook 7H9 supplemented with 0.03% casitone, 0.4% glucose, and 0.05% tyloxapol [41]. Cultures were diluted 1:500 prior to inoculation into the MIC assay. The compounds to be tested were reconstituted to a concentration of 10 mM in DMSO. Two-fold serial dilutions of the test compound were prepared across a 96-well microtitre plate, after which 50 μL of the diluted *M. tuberculosis* cultures were added to each well in the serial dilution. The plate layout was a modification of the method previously described [41]. Assay controls used were a minimum growth control (Rifampicin at 2 × MIC), and a maximum growth control (5% DMSO). The microtitre plates were sealed in a secondary container and incubated at 37°C with 5% CO_2 and humidification. Relative fluorescence (excitation 485 nM; emission 520 nM) was measured using a plate reader (FLUOstar OPTIMA, BMG LABTECH, Ortenberg, Germany) at day 14. The raw fluorescence data were archived and analyzed using the CDD Vault from Collaborative Drug Discovery, in which data were normalized to the minimum and maximum inhibition controls to generate a dose response curve (% inhibition) using the Levenberg–Marquardt damped least squares method, from which the MIC_{90} was calculated (Burlingame, CA, USA, www.collaborativedrug.com). The lowest concentration of drug that inhibited growth of more than 90% of the bacterial population was considered the MIC_{90}.

3.3 | *In silico* Molecular docking studies

The X-ray crystal structure (PDB code: 1C17) [42] was obtained from the Research Collaboratory for Structural Bioinformatics (RCSB) protein data bank (PDB). The ligands were prepared for docking with Ligprep form Schrödinger [43] suite with OPLS3e force field and Epik by adding appropriate hydrogens, and generating possible ionization states and tautomers. Receptor-ligand docking was also carried out in Maestro with glide [44] using SP (Standard precision) with flexible ligands. ADME calculations were carried out with QikProp form Schrödinger suite [43].

4 | CONCLUSIONS

In summary, this paper is reporting a focused library of easily accessible arylquinolinecarboxamides bearing 2-methoxyquinoline core specifically intended for growth inhibition of *Mtb*. All the synthesized derivatives were fully characterized by routine spectroscopic methods such as FT-IR, mass and NMR (^{1}H, ^{13}C). However, *albeit* not impressive, modest anti-*Mtb* activity against drug susceptible *Mtb* H37Rv was observed. Compounds **10** and **11** with methyl substitution at position 6 of the quinoline ring showed promising inhibition with $MIC_{90} = 32.5$ and 40.3 μM, respectively. The preliminary structure–activity relationship data revealed that a methyl moiety at position 6 of the quinoline ring favors anti-*Mtb* activity over methoxy and fluoro substituents. Introducing *para* bromo benzamides at the side chain attached to position 3 of the quinoline ring influence positively the biological activity of the series against *Mtb* H37Rv. Furthermore, we conducted *in silico* docking studies of the synthesized compounds and bedaquiline against *Mtb*ATPase to determine their potential to interfere with the mycobacterial adenosine triphosphate (ATP) synthase. Despite weak antimycobacterial activity, *in silico* ADME prediction and drug-likeliness of the series suggested that these compounds are exhibiting acceptable ADME and physicochemical properties. Further optimization and strategic modification of the score scaffold with respect to introduction of alternative functionalities such as electron withdrawing and lipophilic alkyl groups of varying sizes in the molecular structure could lead to new potent antimycobacterial derivatives. Thus, these research findings emanating from this study are likely to make desirable contribution for future development of diarylquinoline-based antitubercular lead molecules.

ACKNOWLEDGMENTS

The authors acknowledge the financial support for the research by the Thuthuka National Research Foundation (SDK, Grant No. 107270), Rhodes University Sandisa Imbewu Fund (SDK). The *Mtb* screening work was conducted with the financial support of South African Medical Research Council (SAMRC) with funds from National Treasury under its Economic Competitiveness and Support Package, the MMRU (UCT) through the Strategic Health Innovation Partnerships (SHIP) initiative. FRBB was supported by the Malawi Government Scholarship Fund through the University of Malawi.

DATA AVAILABILITY STATEMENT

The data that supports the findings of this study are available in the supplementary material of this article. Target compounds can be obtained from corresponding authors on request.

ORCID

Fostino R. B. Bokosi https://orcid.org/0000-0002-7923-3709
Richard M. Beteck https://orcid.org/0000-0002-6282-043X
Digby F. Warner https://orcid.org/0000-0002-4146-0930
Tendamudzimu Tshiwawa https://orcid.org/0000-0002-2747-1406
Setshaba D. Khanye https://orcid.org/0000-0003-0725-5738

REFERENCES

[1] WHO, World Tuberculosis Report, **2020**.
[2] V. Lohrasbi, M. Talebi, A. Z. Bialvaei, L. Fattorini, M. Drancourt, M. Heidary, D. Darban-Sarokhalil, *Tuberculosis* **2018**, *109*, 17.
[3] Z. F. Udwadia, R. A. Amale, K. K. Ajbani, C. Rodrigues, *Clin. Infect. Dis.* **2012**, *54*, 579.
[4] S. Ahmad, E. Mokaddas, *J. Infect. Public Health* **2014**, *7*, 75.
[5] R. Dua, S. Shrivastava, S.K. Sonwane, S.K. Srivastava, *Adv. Biol. Res.* **2011**, *5*, 120.
[6] K. Andries, P. Verhasselt, J. Guillemont, H. W. Göhlmann, J.-M. Neefs, H. Winkler, J. Van Gestel, P. Timmerman, M. Zhu, E. Lee, *Science* **2005**, *307*, 223.
[7] M. Mirsaeidi, *Int. J. Mycobacteriol.* **2013**, *2*, 1.
[8] S. Parida, R. Axelsson-Robertson, M. Rao, N. Singh, I. Master, A. Lutckii, S. Keshavjee, J. Andersson, A. Zumla, M. Maeurer, *J. Intern. Med.* **2015**, *277*, 388.
[9] M. V. Worley, S. J. Estrada, *Pharmacotherapy* **2014**, *34*, 1187.
[10] N. Lounis, J. Guillemont, N. Veziris, A. Koul, V. Jarlier, K. Andries, *Med. Mal. Infect.* **2010**, *40*, 383.
[11] D. A. Mitchison, *Nat. Biotechnol.* **2005**, *23*, 187.
[12] E. Huitric, P. Verhasselt, K. Andries, S. E. Hoffner, *Antimicrob. Agents Chemother.* **2007**, *51*, 4202.
[13] A. Matteelli, A. C. Carvalho, K. E. Dooley, A. Kritski, *Future Microbiol.* **2010**, *5*, 849.
[14] S. T. Cole, P. M. Alzari, *Science* **2005**, *307*, 214.
[15] E. Segala, W. Sougakoff, A. Nevejans-Chauffour, V. Jarlier, S. Petrella, *Antimicrob. Agents Chemother.* **2012**, *56*, 2326.
[16] P. P. Jain, M. S. Degani, A. Raju, M. Ray, M. G. R. Rajan, *Bioorg. Med. Chem. Lett.* **2013**, *23*, 6097.
[17] G.G. Ladani, M.P. Patel, *New J. Chem.* **2015**, *39*, 9848.
[18] A. Bahuguna, D. S. Rawat, *Med. Res. Rev.* **2020**, *40*, 263.
[19] F. R. B. Bokosi, R. M. Beteck, D. Laming, H. C. Hoppe, T. Tshiwawa, S. D. Khanye, *Arch. Pharm.* **2021**, *354*, e2000331.
[20] F. R. B. Bokosi, R. M. Beteck, M. Mbaba, T. E. Mtshare, D. Laming, H. C. Hoppe, S. D. Khanye, *Bioorg. Med. Chem. Lett.* **2021**, *38*, 127855.
[21] O. Meth-Cohn, B. Narine, B. Tarnowski, *J. Chem. Soc., Perkin Trans. 1* **1981**, 1520. https://doi.org/10.1039/P19810001520
[22] J. T. Kuethe, A. Wong, C. Qu, J. Smitrovich, I. W. Davies, D. L. Hughes, *J. Org. Chem.* **2005**, *70*, 2555.

[23] J. H. Frank, Y. L. Powder-George, R. S. Ramsewak, W. F. Reynolds, *Molecules* **2012**, *17*, 7914.
[24] E. Speri, J. Fishovitz, S. Mobashery, *MedChemComm* **2018**, *9*, 2008.
[25] F. Curreli, H. Zhang, X. Zhang, I. Pyatkin, Z. Victor, A. Altieri, A. K. Debnath, *Bioorg. Med. Chem.* **2011**, *19*, 77.
[26] D. N. Davidson, P. T. Kaye, *J. Chem. Soc., Perkin Trans. 2* **1991**, 927.
[27] W. E. Stewart, T. H. Siddall, *Chem. Rev.* **1970**, *70*, 517.
[28] H. Shanan-Atidi, K. Bar-Eli, *J. Phys. Chem.* **1970**, *74*, 961.
[29] C. B. de Koning, W. A. L. van Otterlo, J. P. Michael, *Tetrahedron* **2003**, *59*, 8337.
[30] Y.-S. Lee, F. G. Siméon, E. Briard, V. W. Pike, *ACS Chem. Neurosci.* **2012**, *3*, 325.
[31] K. C. Sekgota, S. Majumder, M. Isaacs, D. Mnkandhla, H. C. Hoppe, S. D. Khanye, F. H. Kriel, J. Coates, P. T. Kaye, *Bioorg. Chem.* **2017**, *75*, 310.
[32] I. Kehinde, P. Ramharack, M. Nlooto, M. Gordon, *J. Biomol. Struct. Dyn.* **2020**, 1. https://doi.org/10.1080/07391102.2020.1821780
[33] D. Chen, N. Oezguen, P. Urvil, C. Ferguson, S. M. Dann, T. C. Savidge, *Sci. Adv.* **2016**, *2*, e1501240.
[34] G. Bocci, E. Carosati, P. Vayer, A. Arrault, S. Lozano, G. Cruciani, *Sci. Rep.* **2017**, *7*, 6359.
[35] v. QikProp, Schrödinger, LLC, New York, NY, **2015**.
[36] A. I. Vogel, A. R. Tatchell, B. S. Furnis, A. J. Hannaford, P. W. G. Smith, *Vogel's Textbook of Practical Organic Chemistry*, 5th, John Wiley and Sons, New York **1989**.
[37] K.C. Nicolaou, J.A. Pfefferkorn, A.J. Roecker, G.-Q. Cao, S. Barluenga, H.J. Mitchell, *J. Am. Chem. Soc.* **2000**, *122*, 9939.
[38] K. A. Abrahams, J. A. G. Cox, V. L. Spivey, N. J. Loman, M. J. Pallen, C. Constantinidou, R. Fernández, C. Alemparte, M. J. Remuiñán, D. Barros, L. Ballell, G. S. Besra, *PLoS One* **2012**, *7*, e52951.
[39] L. Collins, M. Torrero, S. Franzblau, *Antimicrob. Agents Chemother.* **1998**, *42*, 344.
[40] L. Collins, S. G. Franzblau, *Antimicrob. Agents Chemother.* **1997**, *41*, 1004.
[41] J. J. De Voss, K. Rutter, B. G. Schroeder, H. Su, Y. Zhu, C. E. Barry, *Proc. Natl. Acad. Sci.* **2000**, *97*, 1252.
[42] S. Schrödinger Release 2020–4: Maestro, LLC, New York, NY, **2020**.
[43] S. Schrödinger Release 2020–1: LigPrep, LLC, New York, NY, **2020**.
[44] R. A. Friesner, J. L. Banks, R. B. Murphy, T. A. Halgren, J. J. Klicic, D. T. Mainz, M. P. Repasky, E. H. Knoll, M. Shelley, J. K. Perry, D. E. Shaw, P. Francis, P. S. Shenkin, *J. Med. Chem.* **2004**, *47*, 1739.

SUPPORTING INFORMATION

Additional supporting information may be found online in the Supporting Information section at the end of this article.

How to cite this article: F. R. B. Bokosi, R. M. Beteck, A. Jordaan, R. Seldon, D. F. Warner, T. Tshiwawa, K. Lobb, S. D. Khanye, *J. Heterocycl. Chem.* **2021**, 1. https://doi.org/10.1002/jhet.4340